R-matrix and dynamical model calculations of three-body resonance decay widths

A. J. Bartlett and J. A. Tostevin
Department of Physics, Faculty of Engineering and Physical Sciences, University of Surrey, Guildford, Surrey GU2 7XH, United Kingdom

I. J. Thompson
Lawrence Livermore National Laboratory, Physical Science Directorate, P. O. Box 808, L-414, Livermore, California 94551, USA
(Received 30 August 2008; published 10 November 2008)

Calculations of the decay widths of three-body resonances are considered using both *R*-matrix and dynamical three-body theoretical models. The *R*-matrix approach, which treats the three-body decay as two, ordered two-body decays, has both simultaneous and sequential particle emission pathways, each with an associated decay width. The question of how these two widths should be combined to determine the total resonance width is considered using comparisons with the width deduced from fully dynamical three-body model calculations. We use the decay of the well-understood ^{6}He(2^+, 1.8 MeV) resonance (into $^4\mathrm{He} + n + n$) as a benchmark case.

DOI: 10.1103/PhysRevC.78.054603 PACS number(s): 21.10.Tg, 21.45.−v, 24.30.Gd, 27.20.+n

I. INTRODUCTION

An understanding of the formation and decay of three-body resonance states is of increasing importance as radioactive beam experiments push the boundaries of the detection of bound and resonant states to increasingly exotic nuclei. Two-neutron halo states and two-proton radioactivity are examples of novel three-body phenomena exhibited by such systems.

Traditional *R*-matrix theory [1] assumes that three-body channels make a negligible contribution to decay widths, in comparison with two-body channels, and is not immediately applicable to three-body resonances. However, Lane and Thomas [1] proposed that three-body reactions could be discussed within an *R*-matrix framework if treated as two, ordered two-body reactions. Barker has developed this approach with several applications to two-proton and two-neutron radioactivity [2–5].

Three-body nuclei, composed of A, B, and C, are thus assumed to decay by one of three distinct paths, through intermediate states of the $\{AB\}$, $\{AC\}$, and $\{BC\}$ two-body systems, e.g.,

$$\{ABC\} \rightarrow \{AB\} + C \rightarrow A + B + C,$$

with associated decay widths $\Gamma_{\{AB\}C}$, etc. If these decays are independent then the associated widths should simply be summed to obtain the total three-body decay width of the state $\{ABC\}$. However, as discussed by Barker [5], the decays may not be independent, in which case an estimate of the maximum total width is given by the maximally coherent sum of these partial widths. Barker's analyses found that, in general, the calculated maximally coherent width is less than or equal to the measured widths of the states [5]. Of the nuclei studied by Barker, only one example, the rather broad ^{5}H system, decays by two-neutron emission. In that example it was found that the incoherent sum was in better agreement with experiment, contrary to the findings for the other nuclei. In an attempt to clarify this situation we consider the better understood 2^+(1.8 MeV) three-body resonance in ^{6}He, where the interactions of the two-body subsystems have been studied in some detail. We use a modified version of the approach of Barker [5]. The decay widths obtained are compared with the predictions of full, three-body dynamical calculations, using as nearly as possible the same underlying inputs and interactions. The latter calculations make no assumptions about specific paths of decay.

In the following section the important characteristics of the ^{6}He 2^+ resonance example are discussed. In Sec. III the *R*-matrix approach is introduced very briefly, as it relates to both the two- and three-body systems under discussion. The spectroscopic factors used for the different two-body configurations are also clarified. The parameters and interactions used in the calculations are discussed in Sec. IV. The *R*-matrix model results are then discussed in Sec. V and the three-body model and its results in Sec. VI.

II. THE ^{6}He CASE

The width of the ^{6}He, 2^+(1.8 MeV) resonance was measured [6] to be $\Gamma_{\mathrm{exp}} = 113 \pm 20$ keV. There have also been several theoretical calculations for this system. The results of some of these are summarized in Table I. As is evident from Table I, none of these calculations produce a width consistent with the experiment. Detailed comparisons of the different theoretical predictions are, however, difficult to make. Differences between the various model calculations result from, among other things, the use of different model-space truncations and of different interactions for the system. Further, the latter may or may not have been tuned to position the resonance energy at the measured value. For example, the large width in the case of the algebraic model of Ref. [7] is the result of a 2^+ resonance position at 1.49 MeV (rather than 824 keV) above threshold. In the present work the *R*-matrix description will be compared with three-body calculations based on a hyperspherical harmonics (HH) decomposition of the wave function. Use of the HH method avoids the coherent versus incoherent concerns of the *R*-matrix method, producing the total width of the state directly. The same interactions are used in both calculations, as far as this is possible, to enable fair comparisons.

TABLE I. Previous theoretical calculations of the width of the ^{6}He, 2^+(1.8 MeV) resonance, calculated using the complex scaling (CSM), analytical continuation in the coupling constant (ACCCM), algebraic model (AM) and hyperspherical harmonic (HH) methods. The measured value is also shown.

Γ (keV)	Method	Reference
113 ± 20	Experiment	[6]
60	CSM	[8]
70	ACCCM	[9]
168	AM	[7]
40	HH	[10]
$\sim$60	HH	[11]

In the R-matrix method, the ^{6}He, 2^+(1.8 MeV) decay is via the following ordered two-body routes:

$$\text{I: } {}^6\text{He}(2^+) \rightarrow {}^5\text{He}(3/2^-) + n \rightarrow {}^4\text{He} + n + n,$$
$$\text{II: } {}^6\text{He}(2^+) \rightarrow {}^4\text{He} + {}^2n(0^+) \rightarrow {}^4\text{He} + n + n.$$

Path I decays are referred to as *sequential*, the two neutrons being emitted one after the other. Path II decays are referred to as *simultaneous*, the neutrons being emitted together. Clearly the sequential route requires a knowledge of the $^5\text{He} + n$ and $^5\text{He} = (^4\text{He} + n)$ subsystems and their interactions. The simultaneous route requires consideration of the $^4\text{He} + {}^2n$ and the $n + n$ interactions. Similarly, the three-body HH calculations require, in common, the $^4\text{He} + n$ and $n + n$ interactions. The models used for these interactions are discussed later.

The two decay paths, their associated resonant and virtual state energies, and reaction-relevant decay energies are now defined in Figs. 1 and 2. Here Q_{2n} and Q_{1n} denote the energies of the three-body, ^{6}He(2^+), initial state, and the two-body intermediate resonance/virtual states, respectively, measured relative to the $^4\text{He} + n + n$ threshold. The energies E and U are used to refer to arbitrary energies of the initial (three-body) and intermediate (two-body) systems, respectively. These energies are also measured with respect to threshold.

The R-matrix methodology applied to these two decay pathways is discussed in the following section.

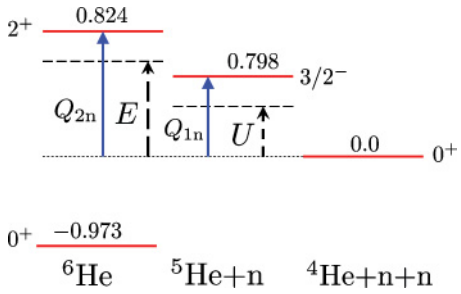

FIG. 1. (Color online) Sequential decay paths from the ^{6}He 2^+ resonance through the unbound intermediate states in ^{5}He. Q_{2n} and Q_{1n}, the energies of the ^{6}He(2^+) and ^{5}He($3/2^-$) resonances relative to threshold, are shown in MeV. The energies E and U refer to arbitrary energies in the initial (^{6}He) and intermediate (^{5}He) systems.

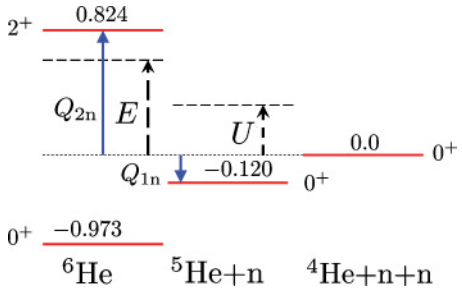

FIG. 2. (Color online) Simultaneous decay paths from the ^{6}He 2^+ resonance through the intermediate, unbound ^2n two-body channels. Q_{2n} and Q_{1n}, the energies of the ^{6}He(2^+) and $^2n(0^+)$ virtual state relative to threshold, are shown in MeV. The energies E and U refer to arbitrary energies in the initial (^{6}He) and intermediate (^2n) systems.

III. THE *R*-MATRIX METHODOLOGY

A. Two-body systems

In two-body R-matrix theory a matching radius, a, marks the boundary between the *internal* ($r \leqslant a$) and *external* ($r > a$) regions of radial separation of the two bodies. In the internal region the exact scattering wave function, $\psi(U, r)$, for a two-body Hamiltonian H at an energy U, is expanded in terms of a complete set of orthonormal R-matrix eigenstates $\tilde{\psi}_p(r)$ as

$$\psi(U, r) = \sum_p C_p \tilde{\psi}_p(r), \quad r \leqslant a, \tag{1}$$

with expansion coefficients C_p. Here, the appropriate orbital and total angular momentum labels of the channel of interest are assumed but are not shown explicitly. The $\tilde{\psi}_p(r)$, with energy eigenvalues ϵ_p, are the solutions of the eigenvalue problem for the same two-body Hamiltonian as calculates $\psi(U, r)$ but subject to the (R-matrix) boundary conditions of (a) regularity at $r = 0$ and (b) the logarithmic derivative condition at $r = a$,

$$\left[\frac{1}{\tilde{\psi}_p(r)}\frac{d\tilde{\psi}_p}{dr}\right]_{r=a} = \beta \tag{2}$$

for a fixed β. Fixing β renders the kinetic energy operator Hermitian on the interval $0 \leqslant r \leqslant a$ and ensures the orthogonality of the states $\tilde{\psi}_p(r)$ in this range. It is usual and convenient to introduce a dimensionless constant $b = a\beta$. This b (with a) determines and will be referred to as the boundary condition.

In the single-term (one-pole) approximation, the scattering wave function is approximated by just the lowest ($p = 1$) normalized R-matrix eigenstate. In this case an optimum choice for b is

$$b = \left[\frac{a}{\psi(E_R, r)}\frac{d\psi(E_R, r)}{dr}\right]_{r=a}, \tag{3}$$

the logarithmic derivative (at $r = a$) of the exact ψ evaluated at the two-body resonance (or virtual state) energy E_R. In the single term limit, we can then drop any reference to p and the R-matrix, $R(U)$, is

$$R(U) = \frac{\gamma^2}{\epsilon - U}, \tag{4}$$

ϵ being the single R-matrix (pole) energy. Here γ^2, the reduced width, is given by [5]

$$\gamma^2 = \frac{\hbar^2}{2\mu a}\mathcal{S}|\tilde{\psi}(a)|^2, \tag{5}$$

where μ is the reduced mass and $\mathcal{S}$ is the spectroscopic factor for the given two-body partition.

B. Spectroscopic factors

In Sec. VI we will discuss dynamical calculations, full continuum solutions of the three-body Schrödinger equation for the $^4\mathrm{He} + n + n$ system, based on use of an HH decomposition of the wave function. Here, to enable best comparisons with the R-matrix analyses, these HH calculations were used to determine the spectroscopic factors, $\mathcal{S}$, for each decay step in the R-matrix calculations—as required for the associated reduced widths in Eq. (5). These HH calculations determine (a) an 84% probability for the $[[^4\mathrm{He} \otimes p_{3/2}]_{3/2^-} \otimes p_{3/2}]_{2^+}$ component of the $^6\mathrm{He}(2^+)$ state. Thus, when multiplied by 2 (the number of valence neutrons), this gives a value $\mathcal{S} = 1.64$ for the $^6\mathrm{He} \to {}^5\mathrm{He} + n$ step, relevant to the sequential decay pathway. Similarly, the $[[^2n(0^+) \otimes (\ell = 2)]_{2^+} \otimes^4 \mathrm{He}]_{2^+}$ probability is 39% and $\mathcal{S} = 0.39$ for the simultaneous, $^6\mathrm{He} \to {}^4\mathrm{He} + {}^2n$ step. The second, implied decay steps, $^2n \to n + n$ and $^5\mathrm{He} \to {}^4\mathrm{He} + n$, are taken to have spectroscopic factors of unity. These spectroscopic factors are collected in Table II.

C. Three-body systems

The three-body decay pathways proceed through an intermediate state, being the $^5\mathrm{He}(3/2^-)$ and $^2n(0^+)$ channels, which include the ^{5}He(g.s.) resonance and the $n + n$ virtual states, respectively. These states are rather broad in their strength with respect to the two-body relative energy variable U (of Figs. 1 and 2). This strength distribution is described by a probability density function, $\rho(U)$. Following Lane and Thomas [1], one can define $\rho(U)$ as the interior norm (IN) of the exact scattering wave function $\psi(U, r)$ at each energy U, i.e.,

$$\rho_{IN}(U) = \int_{r=0}^{a} |\psi(U, r)|^2 dr, \tag{6}$$

where, to maintain consistency with Lane and Thomas, we adopt the asymptotic normalizations

$$\psi(U, r) = \frac{i}{v^{1/2}}[H_\ell^-(kr) - \mathsf{S}_{j\ell} H_\ell^+(kr)]. \tag{7}$$

TABLE II. Spectroscopic factors $\mathcal{S}$, from the HH calculations, as used for the sequential and simultaneous decay pathways from the 2^+(1.8 MeV) resonance in ^{6}He.

Sequential		Simultaneous	
$^6\mathrm{He} \to {}^5\mathrm{He} + n$	$^5\mathrm{He} \to {}^4\mathrm{He} + n$	$^6\mathrm{He} \to {}^4\mathrm{He} + {}^2n$	$^2n \to n + n$
1.64	1.00	0.39	1.00

Because, for ^{6}He, the decays involve only neutrons, the $H_\ell^\pm$ are Hankel functions. v and k are the velocity and wave number corresponding to relative energy U and the $\mathsf{S}_{j\ell}$ are the partial wave S-matrix elements. For a single channel, and in the single term approximation, $\rho(U)$ can be written in the Lane and Thomas (LT), resonance-like form [1]

$$\rho_{\mathrm{LT}}(U) = c\frac{\Gamma_2(U)}{[U - Q_{1n} - \Delta_2(U)]^2 + [\Gamma_2(U)]^2/4}. \tag{8}$$

Here the subscripts 2 refer to the second step of the decay, which for the simultaneous case is $^2n \to n + n$ and for the sequential case is $^5\mathrm{He} \to {}^4\mathrm{He} + n$. The overall multiplicative constant c is chosen such that, when integrated over all U, $\rho(U)$ is normalized to unit strength. This normalization implies that the intermediate state decays proceed with certainty subsequent to their production in the first step. In the following, integrals over U are evaluated on the range 0–10 MeV for the sequential pathway and on 0–20 MeV for the simultaneous pathway. The formal width, $\Gamma_2(U)$, of the second step at energy U is

$$\Gamma_2(U) = 2\gamma_2^2 P_2(U), \tag{9}$$

where $P_2(U)$ is the penetrability,

$$P_2(U) = \frac{ka}{G_\ell(ka)^2 + F_\ell(ka)^2}. \tag{10}$$

Also present in Eq. (8) is the shift term $\Delta_2(U)$, involving the reduced widths. Explicitly,

$$\Delta_2(U) = -\gamma_2^2\,[S_2(U) - b]\,, \tag{11}$$

where the shift function $S_2(U)$, like the penetrability, is defined in terms of the regular and irregular free-particle scattering functions F_ℓ and G_ℓ, as

$$S_2(U) = ka\frac{G'_\ell(ka)G_\ell(ka) + F'_\ell(ka)F_\ell(ka)}{G_\ell(ka)^2 + F_\ell(ka)^2}. \tag{12}$$

Here the primes denote derivatives with respect to the arguments of the functions (kr).

D. R-matrix boundary conditions

A consequence of the energy dependencies of the penetrability and shift terms in Eq. (8) is that $\rho_{\mathrm{LT}}(U)$ is not a Lorentzian and hence the formal width $\Gamma_2(U)$ does not trivially determine the width of $\rho_{\mathrm{LT}}(U)$. However, if one approximates the shift function to be linear over the range of U relevant to the resonance strength and uses the first two terms of its Taylor expansion about the resonance position $U = Q_{1n}$ one obtains a form we call the linear approximation (LA) for $\rho(U)$ that more closely approximates a Lorentzian. Explicitly,

$$\rho_{\mathrm{LA}}(U) = c'\frac{\Gamma_2^0(U)}{\left[U - Q_{1n} - \Delta_2^0\right]^2 + \left[\Gamma_2^0(U)\right]^2/4}, \tag{13}$$

which now contains an energy independent shift term

$$\Delta_2^0 = \frac{-\gamma_2^2[S_2(Q_{1n}) - b]}{1 + \gamma_2^2\,\frac{dS_2}{dU}\big|_{U=Q_{1n}}}, \tag{14}$$

together with an *observed width*, $\Gamma_2^0(U)$, given by

$$\Gamma_2^0(U) = \frac{\Gamma_2(U)}{1 + \gamma_2^2 \frac{dS_2}{dU}\big|_{U=Q_{1n}}}. \quad (15)$$

The observed width provides a better approximation to the actual width of the $\rho(U)$ distribution.

In previous works by Barker, the R-matrix boundary condition was fixed at the value $b = S_2(Q_{1n})$. As is clear from Eq. (14), this choice simplifies $\rho_{\rm LA}(U)$, removing the Δ_2^0 shift term. Specifically, one obtains what we will refer to as the Barker form $\rho_B(U)$,

$$\rho_B(U) = c' \frac{\Gamma_2^0(U)}{[U - Q_{1n}]^2 + \left[\Gamma_2^0(U)\right]^2/4}, \quad (16)$$

with $\Gamma_2^0(U)$ the observed width, as given above.

As was discussed in subsection III A, an optimum choice of the derivative boundary condition in the case of the single-pole approximation to the R-matrix is given by Eq. (3). To calculate these b it is first necessary to specify the two-body interactions for the different subsystems. These are introduced in the next subsection. The consistency or otherwise of the $b = S_2(Q_{1n})$ assignment, and the adequacy of the Barker approximation above can then be assessed.

IV. TWO-BODY INTERACTIONS

With the exception of the $n + n$ interaction, the central potentials in all two-body subsystems are taken to have Woods-Saxon [12] forms,

$$V_{\rm ws}(r) = -V_0/[1 + e^{(r-R_0)/a_0}], \quad (17)$$

where V_0 is the depth, R_0 is the radius, and a_0 the diffuseness. The spin-orbit potential is defined by

$$V_{\rm so}(r) = \frac{-V_{\rm so}}{a_{\rm so} r} \frac{e^{(r-R_{\rm so})/a_{\rm so}}}{[1 + e^{(r-R_{\rm so})/a_{\rm so}}]^2}. \quad (18)$$

We use the following two-body potential parameters. For the sequential paths we need ^{4}He $+ n$ and ^{5}He $+ n$ interactions. For the ^{4}He $+ n$ system, we use the analysis of Bang and Gignoux [13]. There, earlier $p_{3/2}$, $p_{1/2}$, and $s_{1/2}$ ^{4}He $+ n$ phase-shift data were fitted using a Woods-Saxon plus spin-orbit potential. Taking as fixed the geometry of the Bang and Gignoux potential, the program SFRESCO [14] was used to search the depths, V_0 and $V_{\rm so}$, to fit the more extensive recent phase-shift data [15]. Our improved potential depths are shown in Table III. For the ^{5}He $+ n$ interaction the depth of our ^{4}He $+ n$ potential, described above, was adjusted to place the $p_{1/2}$ ^{5}He $+ n$ S-matrix pole at 0.06 MeV above the ^{5}He(g.s.) energy [16]; see Table III.

For the simultaneous decay paths we need $n + n$ and ^{4}He $+$ ^2n interactions. For the $n + n$ interaction we use a simple Gaussian form, namely

$$V_{nn}(r) = -V_0 \exp[-(r/R_0)^2]. \quad (19)$$

The depth and range, given in Table III, parametrize the low-energy scattering, and the virtual state at -0.12 MeV, of two neutrons in a relative s state [17]. Using this or the more complicated Gogny, Pires, and Tourriel (GPT) $n + n$ interaction [18] made only very minor differences to the results of the three-body (HH) calculation. Thus, the Gaussian parametrization of Eq. (19) was used throughout. To specify the ^{4}He $+ {}^2n$ two-body interaction is clearly a source of greater ambiguity in the simultaneous path of the R-matrix method. We have taken three physical limits for this interaction:

TABLE III. The potential parameters used in the R-matrix and HH calculations. The deduced R-matrix boundary conditions, b, for the two steps of each decay pathway are also tabulated.

System	V_0 (MeV) [a_0 (fm)]	R_0(fm)	$V_{\rm so}$ (MeV) [$a_{\rm so}$ (fm)]	$R_{\rm so}$(fm)	b
$n + {}^4$He	44.21 [0.70]	2.00	38.91 [0.35]	1.50	−0.2
$n + {}^5$He	46.60 [0.70]	2.00	40.00 [0.35]	1.50	−0.9
$n + n$[a]	31.00	1.80			0.27
$^2n + {}^4$He					
Dineutron	71.26 [0.70]	2.00			−1.0
$d + {}^4$He	80.25 [0.65]	1.90			−1.1
Bin	39.75 [1.14]	2.38			−0.9

[a]Note that the $n + n$ potential is of Gaussian form.

(i) We assume a point $^2n(0^+)$, or dineutron, in which case the interaction is twice the central part of the ^{4}He $+ n$ interaction of Table III.

(ii) We take the central part of the phenomenological ^{4}He + deuteron cluster model potential, as required to bind ^{6}Li, e.g., Refs. [19,20].
In fact both potentials (i) and (ii) were found to be of the wrong depth, in the sense that they did not generate a ^{6}He (2^+) resonance, for the ^{4}He $+ {}^2n$ system in a relative d wave, at the resonance energy of 0.824 MeV above threshold. The dineutron potential was too deep and the deuteron potential too shallow. The two potential depths were thus tuned to put the resonance in the right position. The resulting parameters are shown in Table III.

(iii) We describe the ^{4}He $+ {}^2n$ interaction based on the folding of the $n + {}^4$He interactions with an extended, normalized continuum bin relative motion wave function for the two neutrons interacting via the Gaussian $n + n$ potential described above. The relative s-wave bin state wave function, $\phi_{\rm nn}(r)$, was constructed with $n + n$ relative energies from 0 to 2 MeV. Thus, $V_{\rm bin}$ is

$$V_{\rm bin}(r) = \langle \phi_{\rm nn} | V_{n\alpha}(r_1) + V_{n\alpha}(r_2) | \phi_{\rm nn} \rangle, \quad (20)$$

where r_1 and r_2, are the two $n + {}^4$He separations. For convenience this bin potential was fitted with a Woods-Saxon form, Table III, and its depth was adjusted as discussed above to position the ^{4}He $+ {}^2n$ resonance in relative d waves. As is evident from Table III these three potentials give a range of potential geometries and will allow an assessment

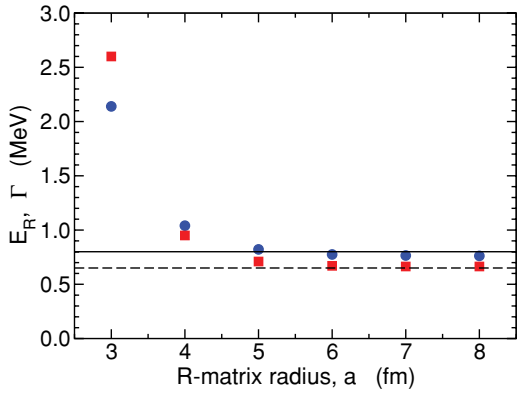

FIG. 3. (Color online) Calculated ^{5}He($3/2^-$) channel resonance energy E_R (closed circles), from the S-matrix pole position, and width Γ (closed squares) as a function of the assumed R-matrix matching radius a. The horizontal lines show the values of E_R (solid line) and Γ (dashed line) of the analysis of Ref. [16].

of the sensitivity to this R-matrix input. Clear also is that the dineutron interaction is the limiting potential for a maximally spatially correlated $n+n$ pair, with $|\phi_{\rm nn}|^2 = \delta(\mathbf{r})$ in Eq. (20).

V. R-MATRIX MODEL RESULTS

We first return to our discussion of the R-matrix boundary conditions of subsection III D. As was discussed there, in the one-term approximation the choice of the derivative boundary condition b affects the form of the $\rho(U)$. The optimum choice of b in this case was stated in Eq. (3).

We used the value $a = 7$ fm for all two-body systems, except $n+n$ for which $a = 5$ fm. These values were chosen such that we obtained converged (with a) S-matrix pole positions in the complex energy plane for the ^{5}He($3/2^-$) channel resonance and for the $n+n$ virtual state. For example, Fig. 3 shows the convergence of the calculated resonance energy E_R (closed circles) and width Γ of the ^{5}He($3/2^-$) ground state as a function of the assumed channel radius. The optimal b were determined (for each two-body interaction) from $\psi(E_R, r)$, with E_R the (real part of the) energy of the appropriate S-matrix pole, located precisely through scans of the complex energy (and/or k) plane. For the ^{4}He $+ n$ interaction $E_R = 0.77$ MeV above threshold and $b = -0.2$. The s-wave virtual state pole of the $n+n$ interaction had $E_R = -0.121$ MeV and $b = 0.27$. Table IV shows that, for both our sequential and simultaneous decays, this optimal b is significantly different from the $b = S_2(Q_{1n})$ Barker choice.

TABLE IV. Comparison of the boundary conditions b for the ^{4}He $+ n$ and the $n+n$ systems calculated from the exact wave functions using Eq. (3) with the values of $S_2(Q_{1n})$, as required for calculations of the probability density functions $\rho(U)$ for the sequential and simultaneous decays, respectively.

Decay route	First step	$S_2(Q_{1n})$	b
Sequential	^{4}He $+ n$	-0.4	-0.2
Simultaneous	$n+n$	-0.3	0.27

This choice should be a good approximation to the optimum b in cases where the hard-sphere phase shifts are effectively constant for the U values across the resonances of interest. The values of Table IV show clearly that the values of b and $S_2(Q_{1n})$ need to be maintained independently and hence that the use of $\rho_B(U)$ is inappropriate in the present case.

The ^{5}He $+ n$ potential, tuned for the ^{6}He (2^+) resonance pole at $E_R = 0.059$ MeV above the ^{5}He(g.s.), had $b = -0.9$. The three model ^{4}He $+ ^2n$ interactions, all tuned to place the ^{6}He 2^+ resonant S-matrix pole at $E_R = 0.944$ MeV above the $n+n$ virtual state, gave boundary conditions $b = -1.0, -1.1$, and -0.9 for the point dineutron, ^{4}He $+ d$, and the bin potentials, respectively. All b are collected in Table III.

A. Probability density functions

Figure 4 shows the ^{5}He probability density functions $\rho(U)$ calculated directly from the interior norm of the scattering wave function (IN), Eq. (6), the Lane and Thomas form (LT), Eq. (8), and the linear approximation (LA), Eq. (13). The IN curve exhibits a high-energy tail, absent from the LT and LA approximations, attributable to the use of the single-pole approximation in the formulation of the latter. Having omitted the $p > 1$ poles and normalized $\rho(U)$ to unity, we have forced the decay through the resonance without the higher-energy pole contributions.

Figure 5 shows the calculated $n+n$ probability density functions for the simultaneous decay route. The figure shows the failure of the linear approximation (LA), Eq. (13), in this case compared to the $\rho_{\rm IN}$ calculated directly from the scattering wave functions, Eq. (6). This is not unexpected. Because for relative s waves the shift function is negative for negative U and vanishes for positive U, the linear (Taylor) approximation about $Q_{1n} = -0.121$ MeV is a poor representation for all positive U. In the s-wave $n+n$ case, a better approximation is to set the shift function to zero, which we denote $\rho_{\rm ZS}(U)$. In this case

$$\rho_{\rm ZS}(U) = c\frac{\Gamma_2(U)}{\left(U - Q_{1n} - \gamma_2^2 b\right)^2 + [\Gamma_2(U)]^2/4}. \qquad (21)$$

This is also shown in Fig. 5.

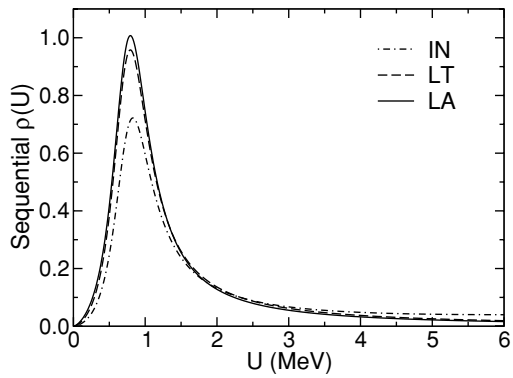

FIG. 4. The calculated ^{5}He probability density functions for the sequential decay route using the interior norm (IN), Lane and Thomas (LT) and linear approximation (LA) schemes for $\rho(U)$. All functions are normalized to unity on the U interval from 0 to 10 MeV.

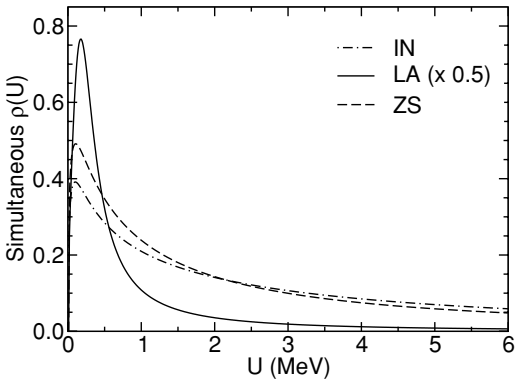

FIG. 5. The calculated $n+n$ probability density functions for the simultaneous decay route using the interior norm (IN), the linear approximation (LA) and the zero-shift function approximation (ZS), Eq. (21), schemes for $\rho(U)$. All functions are normalized to unity on the U interval from 0 to 20 MeV.

B. Sequential, simultaneous, and total widths

The total *observed widths*, $\Gamma^0_{\rm tot}$, of each of the decay pathways taken individually, from an initial state with three-body energy E above threshold, is given (see, e.g., Ref. [5]) by the weighted integral over intermediate state energies

$$\Gamma^0_{\rm tot}(E) = \int_0^E \Gamma^0_1(E,U)\rho(U)dU. \tag{22}$$

Here, subscript 1 now indicates quantities associated with the first step of the decay that is $^6\mathrm{He} \to {}^5\mathrm{He} + n$ (sequential) and $^6\mathrm{He} \to {}^4\mathrm{He} + {}^2n$ (simultaneous) and the observed width of the first step, Γ^0_1, having made the linear approximation, is

$$\Gamma^0_1(E,U) = \frac{\Gamma_1(E,U)}{1+\gamma_1^2\int_0^\infty [dS_1(E-U)/dE]_{E=Q_{2n}}\rho(U)dU}. \tag{23}$$

The formal width of the first step, Γ_1, is

$$\Gamma_1(E,U) = 2\gamma_1^2 P_1(E-U). \tag{24}$$

All elements of these formulas have been defined previously. We calculate the widths $\Gamma^0_{\rm tot}(Q_{2n})$ where the three-body energy is that of the $^6\mathrm{He}(2^+)$ resonance, 0.824 MeV. The calculations presented below used $\rho_{\rm LA}(U)$ and $\rho_{\rm ZS}(U)$ for the sequential and simultaneous paths, respectively.

Table V shows the total R-matrix widths for the sequential and simultaneous paths. The sequential width, $\Gamma^0_{\rm seq} = 34.8$ keV, is more than a factor of 3 greater than our largest estimate of the simultaneous width. Thus, we can already conclude that the sequential route is the dominant decay

TABLE V. Sequential and simultaneous widths (in keV) for the decay of the $^6\mathrm{He}(2^+)$ resonance. These widths were calculated using $\rho_{\rm LA}(U)$ for the sequential path and $\rho_{\rm ZS}(U)$ for the simultaneous path.

	Sequential	Simultaneous		
		Dineutron	$^4\mathrm{He}+d$	Bin
$\Gamma^0_{\rm tot}$ (keV)	34.8	4.29	3.54	11.2

TABLE VI. Coherent and incoherent sums of the sequential and simultaneous decay widths, Eq. (25), for the $^6\mathrm{He}, 2^+(1.8$ MeV) resonance. Results are shown for the three $^4\mathrm{He}+{}^2n$ potential models discussed.

Potential	$\Gamma_{\rm inc}$ (keV)	$\Gamma_{\rm coh}$ (keV)
Dineutron	39.1	63.5
$^4\mathrm{He}+d$	38.4	60.6
Bin	46.0	85.4

mechanism. For the simultaneous path, the point dineutron and $^4\mathrm{He}+d$ potentials give smaller widths than the bin potential. We observe a significant correlation between the simultaneous widths and the depth and diffuseness of the assumed $^4\mathrm{He}+{}^2n$ interaction. Neither of the two separate widths is comparable to the $\Gamma_{\rm exp} = 113 \pm 20$ keV value. Their combination, and possible coherence, is therefore an important issue.

In the conventional two-body R-matrix theory [1], partial widths of different decay channels, c, are simply summed (incoherently) to $\Gamma_{\rm inc}$. However, as was discussed by Barker [5], combining partial widths of three-body decay paths is less clear. Allowing for interference between the channels, the maximum possible (coherent) total width $\Gamma_{\rm coh}$ is the maximally coherent sum. These are:

$$\Gamma_{\rm inc} = \sum_c \Gamma^0_c, \quad \Gamma_{\rm coh} = \left[\sum_c (\Gamma^0_c)^{1/2}\right]^2. \tag{25}$$

Table VI shows the $\Gamma_{\rm inc}$ and $\Gamma_{\rm coh}$ resulting from the $^6\mathrm{He}$ decay paths, calculated using the three model $^4\mathrm{He}+{}^2n$ potentials. The maximally coherent sum is in better agreement with $\Gamma_{\rm exp}$. This result is in agreement with the findings of Barker in the majority of cases studied, e.g., Ref. [5].

VI. THREE-BODY DYNAMICAL CALCULATIONS

Only the most pertinent points and parameters of these three-body calculations are discussed here. The details of the HH technique for the solution of the three-body problem can be found in Refs. [21–23]. The model calculations were performed using the programs EFADDY [24] and STURMXX [25] developed by Thompson *et al*. The three-body HH calculations use the same fixed $n+n$ and $^4\mathrm{He}+n$ potentials as in the R-matrix calculations. In addition, however, the HH model also includes a small, central hyperradial three-body potential, V_{3B}, of the form [21],

$$V_{3B}(\rho_r) = V^0_{3B}/[1+(\rho_r/\rho_0)^3]. \tag{26}$$

This potential, a function only of the hyperradius, ρ_r, has a range determined by ρ_0. This value is typically of order 5 fm. This range having been fixed, the depth, V^0_{3B} was tuned to place the $^6\mathrm{He}(2^+)$ state at 0.824 MeV to ensure fair comparison with the R-matrix results. Pauli blocking of occupied core states was taken into account using (i) a repulsive potential in the s-wave $^4\mathrm{He}+n$ subsystem and (ii) Pauli projection operators [23], which project the forbidden states to a large positive energy. The results using the two methods agreed within 1%. Using the HH terminology [25], a maximum hypermomentum

of $K_{\max} = 30$, a maximum hyperradius $\rho_{\max} = 30$ fm and a maximum number of basis functions of $Q = 25$ were sufficient to obtain converged HH calculations in the ^{6}He(2^+) case. For these converged calculations the value of V_{3B}^0 is -0.34 MeV.

The three-body decay width, Γ_{3B}, was extracted here from the HH calculations through the sum of the eigenphases, $\delta_k(E)$. These were calculated from the eigenvalues $S_k(E) = \exp[2i\delta_k(E)]$ of the unitary, multichannel S-matrix. Following Hazi [26], the width is then extracted from the sum of the eigenphases, $\Delta(E) = \sum_k \delta_k(E)$ by use of the usual resonance relationship,

$$\frac{2}{\Gamma_{3B}} = \left.\frac{d\Delta(E)}{dE}\right|_{Q_{2n}}. \tag{27}$$

The total three-body width calculated this way is $\Gamma_{3B} = 71.6$ keV; however this value is rather robust when obtained from different prescriptions. The 2^+ channel strength distributions in the region of the 2^+ resonance, calculated using three methods, are shown in Fig. 6 as a function of the three-body energy E of the $^4\text{He} + n + n$ system. The curves show the distributions calculated using (a) the derivatives of the sum of the eigenphases, of Eq. (27) above, with the solid points and dashed curve, (b) the interior norms (for radii less than 10 fm) of the three-body wave functions with the dot-dashed curve, and (c) the $B(E2)$ strength distribution (per MeV) for electromagnetic excitations of the 2^+ continuum from the ^{6}He ground-state with the solid curve. As is clear, the deduced widths from these three approaches are in good agreement.

A. Comparison with the *R*-matrix sequential width

As a further comparison to the R-matrix calculations, the HH method was used to obtain an estimate of the sequential width. To suppress the simultaneous path the $n + n$ potential was removed from the calculation. To maintain the 2^+ resonance at the correct energy, and to exclude $n + n$ correlations at large distance, the three-body interaction was also adjusted. Specifically, its radius was reduced to $\rho_0 = 2.0$ fm and the strength required was now $V_{3B}^0 = -15.1$ MeV. This returned an estimate for the sequential width of $\Gamma_{\text{seq}} = 46.5$ keV that compares reasonably with the R-matrix sequential width of $\Gamma_{\text{seq}}^0 = 34.8$ keV, given that one cannot fully remove the two-neutron correlations in the three-body framework.

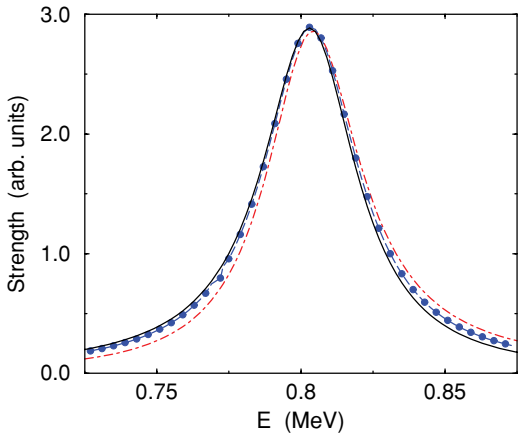

FIG. 6. (Color online) Peaks describing the 2^+ resonance in ^{6}He, from the three-body dynamical calculations. Strength distributions are shown as a function of the three-body energy, E, calculated using (a) the derivatives of the sum of the eigenphases, as given by Eq. (27) (solid points and dashed curve), (b) the interior norms (for radii less than 10 fm) of the three-body dynamical model wave functions (dot-dashed curve), and (c) the $B(E2)$ strength distribution (per MeV) for electromagnetic excitations of the 2^+ continuum from the ^{6}He ground-state (solid curve). All curves have been scaled to the same peak height.

VII. DISCUSSION AND CONCLUSIONS

A summary of the calculated ^{6}He, 2^+(1.8 MeV) three-body resonance widths from the R-matrix and dynamical models is presented in Fig. 7. The experimental value, $\Gamma_{\text{exp}} = 113 \pm 20$ keV is indicated by the solid line and the associated errors by the dashed horizontal lines. As has been made clear, all calculations have had their interactions tuned so as to position the resonance, allowing a direct comparison of the resulting widths. All of the theoretical calculations fall short of the experimental value. The maximally coherent sum of the R-matrix partial widths is in better agreement with the dynamical three-body width. Our R-matrix and dynamical calculation results for the widths agree reasonably well with those examples from the literature that predict the position of the 2^+ resonance appropriately, as are given in Table I. The large width from the algebraic model was discussed already in Sec. II.

In summary, R-matrix and dynamical three-body calculations of the width of the ^{6}He, 2^+(1.8 MeV) three-body resonance were performed. The R-matrix approach treated both the sequential neutron emission and the simultaneous

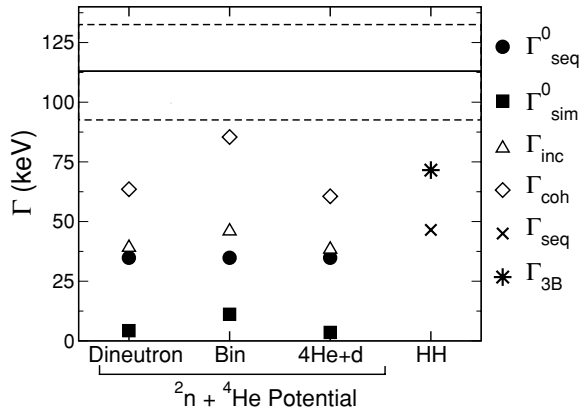

FIG. 7. Comparison of calculated R-matrix and three-body model widths for ^{6}He(2^+). Γ_{seq}^0 and Γ_{sim}^0 are the sequential and simultaneous R-matrix widths. Γ_{inc} and Γ_{coh} are the incoherent and maximally coherent sums of these partial widths. These are shown for the three model $^4\text{He} + {}^2n$ potentials. Γ_{seq} is the estimate of the sequential width from the three-body calculations and Γ_{3B} is the full decay width of the three-body calculations. The measured width is indicated by the solid horizontal line, with its error bars shown by the dashed horizontal lines.

two-neutron emission decay pathways. The sequential decay was found to be dominant with a width in excess of three times that for the simultaneous process for all of the model two-body interactions used. Agreement between the two sets of calculations is reasonable if one assumes maximal coherence between the R-matrix partial widths for the sequential and simultaneous decay paths. Like earlier theoretical approaches, the decay widths resulting from both sets of calculations fall short of the experimentally measured width.

ACKNOWLEDGMENTS

This work was performed under the auspices of the U.S. Department of Energy by Lawrence Livermore National Laboratory under contract DE-AC52-07NA27344, and with the financial support of the United Kingdom Science and Technology Facilities Council (STFC) under grant no. EP/D003628. A.J.B. acknowledges the support of the United Kingdom Engineering and Physical Sciences Research Council (EPSRC).

[1] A. M. Lane and R. G. Thomas, Rev. Mod. Phys. **30**, 257 (1958).
[2] F. C. Barker, Phys. Rev. C **59**, 535 (1999).
[3] F. C. Barker, Phys. Rev. C **63**, 047303 (2001).
[4] F. C. Barker, Phys. Rev. C **66**, 047603 (2002).
[5] F. C. Barker, Phys. Rev. C **68**, 054602 (2003).
[6] F. Ajzenberg-Selove, J. W. Watson, and R. Middleton, Phys. Rev. **139**, B592 (1965).
[7] V. Vasilevsky, A. V. Nesterov, F. Arickx, and J. Broeckhove, Phys. Rev. C **63**, 034607 (2001).
[8] A. Csótó, Phys. Rev. C **49**, 3035 (1994).
[9] N. Tanaka, Y. Suzuki, and K. Varga, Phys. Rev. C **56**, 562 (1997).
[10] B. V. Danilin and M. V. Zhukov, Physics of Atomic Nuclei **56**, 460 (1993).
[11] S. N. Ershov, B. V. Danilin, and J. S. Vaagen, Phys. Rev. C **64**, 064609 (2001).
[12] R. D. Woods and D. S. Saxon, Phys. Rev. **95**, 577 (1954).
[13] J. M. Bang and C. Gignoux, Nucl. Phys. **A313**, 119 (1979).
[14] I. J. Thompson, Program FRESCO, available from: www.fresco.org.uk.
[15] J. E. Bond and F. W. K. Firk, Nucl. Phys. **A287**, 317 (1977).
[16] D. R. Tilley, C. M. Cheves, J. Godwin, G. M. Hale, H. M. Hoffman, J. H. Kelley, C. G. Sheu, and H. R. Weller, Nucl. Phys. **A708**, 3 (2002).
[17] L. Johannsen, A. S. Jensen, and P. Hansen., Phys. Lett. **B244**, 357 (1990).
[18] D. Gogny, P. Pires, and R. Tourriel, Phys. Lett. **B32**, 591 (1970).
[19] H. Nishioka, J. A. Tostevin, and R. C. Johnson, Nucl. Phys. **A415**, 230 (1984).
[20] H. Ohnishi, M. Tanifuji, M. Kamimura, Y. Sakuragi, and M. Yahiro, Nucl. Phys. **A415**, 271 (1984).
[21] B. V. Danilin, I. J. Thompson, J. Vaagen, and M. V. Zhukov, Nucl. Phys. **A632**, 383 (1998).
[22] M. A. Khan, S. K. Dutta, T. K. Das, and M. K. Pal, J. Phys. G: Nucl. Part. Phys. **24**, 1519 (1998).
[23] I. J. Thompson, B. V. Danilin, V. D. Efros, J. S. Vaagen, J. M. Bang, and M. V. Zhukov, Phys. Rev. C **61**, 024318 (2000).
[24] I. J. Thompson *et al.*, Program EFADDY, available from: www.fresco.org.uk/programs/efaddy/index.html.
[25] I. J. Thompson, Program STURMXX, available from: www.fresco.org.uk/programs/sturmxx/index.html.
[26] A. U. Hazi, Phys. Rev. A **19**, 920 (1979).